Electrochimica Acta 389 (2021) 138638

Contents lists available at ScienceDirect

Electrochimica Acta

journal homepage: www.elsevier.com/locate/electacta

Ni-modified $Fe_3O_4(001)$ surface as a simple model system for understanding the oxygen evolution reaction

Francesca Mirabella[a,+,#,*], Matthias Müllner[a,+], Thomas Touzalin[b,+], Michele Riva[a], Zdenek Jakub[a], Florian Kraushofer[a], Michael Schmid[a], Marc T.M. Koper[b], Gareth S. Parkinson[a], Ulrike Diebold[a,*]

[a] Institut für Angewandte Physik, Technische Universität Wien, A-1040 Wien, Austria
[b] Leiden Institute of Chemistry, Leiden University, PO Box 9502, 2300 RA, Leiden, The Netherlands

ARTICLE INFO

Article history:
Received 26 February 2021
Revised 7 May 2021
Accepted 15 May 2021
Available online 20 May 2021

Keywords:
OER
Fe-Ni oxides
surface science
electrochemistry
water splitting

ABSTRACT

Electrochemical water splitting is an environmentally friendly technology to store renewable energy in the form of chemical fuels. Among the earth-abundant first-row transition metal-based catalysts, mixed Ni-Fe oxides have shown promising performance for effective and low-cost catalysis of the oxygen evolution reaction (OER) in alkaline media, but the synergistic roles of Fe and Ni cations in the OER mechanism remain unclear. In this work, we report how addition of Ni changes the reactivity of a model iron oxide catalyst, based on Ni deposited on and incorporated in a magnetite $Fe_3O_4(001)$ single crystal, using a combination of surface science techniques in ultra-high vacuum such as low energy electron diffraction (LEED), x-ray photoelectron spectroscopy (XPS), low-energy ion scattering (LEIS), and scanning tunneling microscopy (STM), as well as atomic force microscopy (AFM) in air, and electrochemical methods such as cyclic voltammetry (CV) and electrochemical impedance spectroscopy (EIS) in alkaline media. A significant improvement in the OER activity is observed when the top surface presents an iron fraction among the cations in the range of 20-40%, which is in good agreement with what has been observed for powder catalysts. Furthermore, a decrease in the OER overpotential is observed following surface aging in electrolyte for three days. At higher Ni load, AFM shows the growth of a new phase attributed to an (oxy)-hydroxide phase which, according to CV measurements, does not seem to correlate with the surface activity towards OER. EIS suggests that the OER precursor species observed on the clean and Ni-modified surfaces are similar and Fe-centered, but form at lower overpotentials when the surface Fe:Ni ratio is optimized. We propose that the well-defined $Fe_3O_4(001)$ surface can serve as a model system for understanding the OER mechanism and establishing the structure-reactivity relation on mixed Fe-Ni oxides.

© 2021 The Author(s). Published by Elsevier Ltd.
This is an open access article under the CC BY-NC-ND license
(http://creativecommons.org/licenses/by-nc-nd/4.0/)

1. Introduction

Currently most energy sources used by our society are based on fossil fuels. Their combustion (coal, oil, and gas), together with large-scale deforestation, is causing massive emissions of greenhouse gases. Given the destructive environmental impact of these gases, effort has focused on the production, storage and transport of renewable energy (wind or sunlight) [1]. A promising technology to address this issue uses renewable energy to produce chemical energy through the splitting of water into hydrogen and oxygen (water electrolysis) [2]. However, the efficiency of the electrolysis process is hampered by the sluggish kinetics of water oxidation to O_2, also known as oxygen evolution reaction (OER). This reaction has been described as the bottleneck of the water splitting and understanding its mechanism at the atomic scale could be a first step in addressing this challenge [2]. Many catalysts have been proposed to reduce the overpotential losses for OER and investigated in different pH conditions [3], from acidic ($2H_2O \rightarrow 4H^+ + O_2 + 4e^-$) to alkaline ($4OH^- \rightarrow 2H_2O + O_2 + 4e^-$) media. In acidic media, noble metals such as Ru or Ir show promising OER stability and activity.

* Corresponding authors.
+ = These authors contributed equally.
# = Current address: Bundesanstalt für Materialforschung und -prüfung, Unter den Eichen 44-46, 12203 Berlin, Germany.

https://doi.org/10.1016/j.electacta.2021.138638
0013-4686/© 2021 The Author(s). Published by Elsevier Ltd. This is an open access article under the CC BY-NC-ND license
(http://creativecommons.org/licenses/by-nc-nd/4.0/)

However, due to their limited availability and high price many researchers are seeking alternative catalysts based on earth-abundant elements [3,4,5,6,7,8]. In an alkaline environment, oxides and hydroxides of late first-row transition metals (Mn, Fe, Co, Ni) have been found to have comparable performances to noble metals [3]. In particular, NiFe-based (oxy)hydroxide catalysts are reported to show the lowest overpotential for OER in alkaline conditions (pH 13 and 14) [9], but the synergistic role of Fe and Ni is still under debate.

Comparing OER catalysts is complicated by many underlying factors, including differences in electrochemically active surface area, catalyst electrical conductivity, surface chemical stability, surface composition, and reaction mechanism. In this work, we describe our efforts to circumvent these issues by using a combined surface science/electrochemistry approach to develop an atomically controlled model system for the OER on FeNi-based catalysts. Having previously solved the surface structural model for the Fe_3O_4(001) surface [10] and learned how to judiciously alter this surface by doping with nickel atoms [11], we have prepared well-defined Ni-modified Fe_3O_4(001) surfaces in ultra-high-vacuum (UHV) with different Fe:Ni ratios and, after characterization with surface science techniques, we have studied their electrochemical performances towards OER using cyclic voltammetry and electrochemical impedance spectroscopy. A significant increase in the OER activity is observed as the Ni content increases, and the optimum composition has an iron fraction among the cations in the top surface layer in the range of 20-40%. These results are in good agreement with literature for the best OER powder catalysts [9]. Furthermore, based on the analysis of the surface morphological changes before and after reaction, together with adsorption capacitance measurements, we propose that the active sites responsible for the formation of the OER precursor are the same on the clean and on the Ni-modified magnetite. Nevertheless, the presence of the Ni on the surface shifts the formation of this precursor to lower overpotential.

Our study provides a well-defined model catalyst that is at the same time simple, highly active, and stable under operation conditions, and therefore ideal to be used as model system to gain atomic-scale insights into the complicated OER mechanism.

2. Experimental details

2.1. UHV preparation and characterization

The experiments were performed on a natural Fe_3O_4(001) single crystal (SurfaceNet GmbH) prepared in UHV by cycles of 1 keV Ar^+ sputtering and 900 K annealing. Every other annealing cycle was performed in an O_2 environment ($p_{O_2} = 5 \times 10^{-7}$ mbar, 20 min) to maintain the stoichiometry of the crystal selvedge. Surface analysis was performed in a UHV system with a base pressure $<10^{-10}$ mbar, furnished with a commercial Omicron SPECTALEED rear-view optics and an Omicron UHV STM-1. XPS data were acquired using non-monochromated Al Kα x-rays and a SPECS PHOIBOS 100 electron analyser at grazing emission (70° from the surface normal). The same analyser was used to carry out the low-energy He^+ ion scattering (LEIS) experiments (1.225 keV He^+, scattering angle 137°), an exquisitely surface-sensitive technique. For quantification of LEIS data, we assumed that the concentrations are proportional to the peak areas, which is justified due to the very similar cross sections, electronic structure, and work function of these metals. Ni was deposited using a Focus electron-beam evaporator, for which the deposition rates were calibrated using a temperature-stabilized quartz crystal microbalances (QCM). One monolayer (ML) is defined as one atom per ($\sqrt{2} \times \sqrt{2}$)R45° unit cell, which corresponds to 1.42×10^{14} atom/cm^2. Ni depositions higher than 2 ML were prepared by first depositing 2 ML Ni on the surface at room temperature, followed by mild annealing at 200 °C for 10 min. This causes a transition from Ni being present as 2-fold coordinated adatoms to 6-fold coordinated "incorporated" cations [11], see Fig. 1; the procedure was then repeated as many times as necessary to reach the desired coverage.

2.2. In-air characterization

After UHV-preparation and characterization as well as after the electrochemical measurements, the samples were brought to air and imaged using an Agilent 5500 ambient AFM in intermittent contact mode with Si tips on Si cantilevers.

2.3. Electrochemical measurements

Cyclic voltammetry and impedance spectroscopy were performed using a Metrohm-Autolab PGSTAT32 potentiostat and a custom-made electrochemical flow cell (made from perfluoroalkoxy alkane, PFA), mounted to the vacuum chamber. Prior to experiments, the chamber was filled with Ar (99.999%, Air Liquide, additionally purified with Micro-Torr point-of-use purifiers, SAES MC50−902 FV) to ambient pressure. The contact between sample and flow cell was sealed with Kalrez O-rings. Prior to measurements, the electrolyte reservoir was evacuated and ultrasonicated to remove dissolved CO_2. The flow cell was filled with electrolyte by increasing the pressure in the electrolyte compartment with Ar to slight overpressure. A glassy carbon counter electrode and a leak-free Ag/AgCl reference electrode (Innovative Instruments Inc.) were used. For impedance measurements, the latter was coupled to a glassy carbon quasi-reference electrode through a 100 nF capacitor. All electrochemical data were corrected for iR_u drop; the uncompensated solution resistance R_u was determined from impedance Nyquist plots by extrapolating the minimum total impedance in the linear regime between 10 kHz and 100 kHz. All electrochemical potentials are referred to either the measured Ag/AgCl reference electrode $E_{Ag/AgCl}$ or given as the overpotential η, which was determined via the equation $\eta = E_{Ag/AgCl} + E_{RHE} - 1.229$ V $- iR_u$. E_{RHE} is the potential of the reversible hydrogen electrode (RHE) vs a Ag/AgCl electrode. The potential of the RHE (Hydroflex) was measured before and after the electrochemical measurements to improve consistency of the results. The electrolyte was prepared from level-1 water (Merck Milli-Q, ρ= 18.2 MΩ·cm, 3 ppb total organic carbon), and reagent-grade NaOH (50 mass % in water, Sigma-Aldrich). Prior to use, all glassware and PFA parts where cleaned by boiling in 20% nitric acid and copious rinsing with Milli-Q water.

3. Results

3.1. Characterization of the catalyst surface before reaction

Fig. 1a shows a schematic model of the UHV-prepared Fe_3O_4(001) surface. The surface is oxidized with respect to the bulk Fe_3O_4 and is not a simple bulk truncation. Specifically, an interstitial tetrahedrally coordinated iron in the second layer (Fe_{tet}, light blue in the model) replaces two octahedrally coordinated iron atoms (Fe_{oct}, dark blue) in the third layer [10], giving rise to a ($\sqrt{2} \times \sqrt{2}$)R45° periodicity. All surface Fe is in the 3+ state in the so-called subsurface cation vacancy (SCV) reconstruction, and it is the most stable termination of Fe_3O_4(001) over the range of oxygen chemical potentials encountered in UHV-based experiments [10].

In the lower part of Fig. 1a, a typical STM image of the UHV-prepared Fe_3O_4(001) surface is shown. Undulating rows of surface Fe atoms appearing as protrusions run in the [110] direction. It

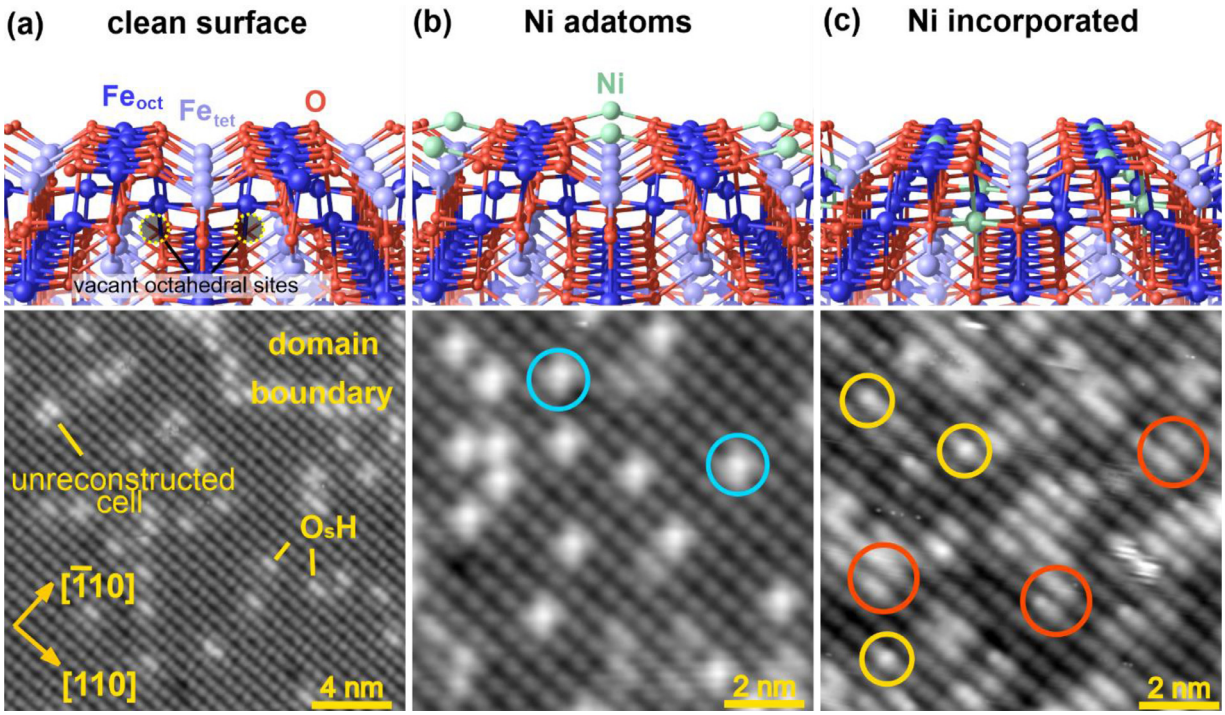

Fig. 1. Atomic models showing side views of the (a) $Fe_3O_4(001)$ clean, (b) doped with 2-fold coordinated Ni adatoms, and (c) with 6-fold coordinated Ni incorporated, as well as corresponding STM images. The clean $Fe_3O_4(001)$ surface in (a) exhibits a $(\sqrt{2} \times \sqrt{2})R45°$ reconstruction due to subsurface cation vacancies (SCV) (octahedrally coordinated Fe_{oct} are dark blue, tetrahedrally coordinated Fe_{tet} are light blue, O atoms are red, and Ni atoms are light green). The STM image below shows the clean surface and its common defects: surface O_sH groups, antiphase domain boundaries and unreconstructed unit cells. In (b) Ni adatoms are adsorbed in the 2-fold-coordinated surface sites, each formed by two undercoordinated O atoms. In the STM image below, the Ni adatoms are highlighted by light blue circles (the Ni coverage is 0.15 ML). In (c) the Ni is incorporated into the subsurface and occupies the vacant octahedral site or replaces a surface Fe_{oct} atom in a metastable configuration. Both types of incorporated Ni are shown in the STM image below, highlighted by red and yellow respectively. (The coverage of the Ni adatoms was 0.40 monolayers (ML) before the incorporation, where 1 ML Ni is defined as one nickel atom per $(\sqrt{2} \times \sqrt{2})R45°$ unit cell or 1.42×10^{14} atoms per cm^2. *This figure is adapted from Ref.* [15].

is common to observe surface hydroxyl groups O_sH (i.e. hydrogen atoms bonding to surface oxygen atoms, which are themselves not imaged) as bright protrusions on the Fe rows. This occurs because the hydroxyl modifies the density of states of the nearby Fe cations, causing them to appear brighter in empty-states STM images [12,13]. Fig. 1a also displays other common defects visible on the clean surface, such as antiphase domain boundaries, which are imaged as meandering line defects, and unreconstructed unit cells, which appear similar to two neighboring hydroxyl groups. These are caused by two additional Fe atoms in the subsurface layer (instead of one interstitial Fe), which again modifies the density of states of the surface atoms [12,14]. It is not possible to image the surface oxygen atoms in STM as they have no density of states in the vicinity of the Fermi level. However, their positions are exactly known from density functional theory calculations and quantitative low-energy electron diffraction (red in model in Fig. 1a) [10].

The surface reconstruction makes it possible to progressively modify the magnetite surface and accommodate foreign metal atoms (such as nickel) in specific positions. [11] Following Ni evaporation under the appropriate temperature conditions, it is possible to obtain two different Ni geometries: Ni adatoms 2-fold coordinated to surface oxygen atoms (model in Fig. 1b, green) and incorporated Ni occupying octahedrally coordinated sites below the surface (model in Fig. 1c) [11,15]. Ni deposition at room temperature leads to Ni adatoms in the 2-fold coordination, which are imaged in STM as isolated, bright protrusions appearing between the Fe rows (light blue circles in Fig. 1b). The transition from 2-fold to 6-fold coordination is achieved by annealing the surface at 200 °C for 10 minutes. As the incorporated Ni atoms are in the subsurface, they cannot be imaged directly in STM, but they modify the electronic structure of the nearby Fe cations, making them to appear brighter in empty-state images (red circles in Fig. 1c) [11,15]. Their appearance is similar to the unreconstructed cell discussed earlier (Fig. 1a). Furthermore, the STM image in Fig. 1c shows additional protrusions within the Fe rows (highlighted with yellow circles), which we previously assigned to Ni replacing Fe atoms in the 5-fold-coordinated position in the top surface layer [15].

The incorporation of Ni in the vacant subsurface octahedral site is only possible if the interstitial Fe_{tet} moves back into the other subsurface octahedral site of the unit cell. The resulting cation rearrangement closely resembles a bulk-truncated $Fe_3O_4(001)$ surface [11,16], and a (1×1) periodicity is observed in LEED. It is possible to recover the clean $(\sqrt{2} \times \sqrt{2})R45°$ reconstructed surface by annealing to high temperatures, which causes the Ni atoms to diffuse into deep bulk layers.

Hereafter, we deal exclusively with the incorporated Ni-doped magnetite shown in Fig. 1c, which resembles the structure of mixed spinel ferrite, i.e., a $Ni_xFe_{3-x}O_4$-like system, suggested to be one of the most active phases in OER [17,18].

The XPS spectra in Fig. 2a shows the Ni *2p* region for different coverages after Ni was deposited onto the $Fe_3O_4(001)$ surface at room temperature and annealed at 200 °C. Five different total Ni depositions are considered: 1 ML (green), 10 ML (purple), 50 ML (blue), 120 ML (pink), and 180 ML (light blue). Corresponding fits for the Ni *2p* peaks are shown in Figure S1 in the supporting information.

After deposition of 1 ML, a small signal is observed in XPS at 855.5 eV, corresponding to the Ni $2p_{3/2}$ peak [19,9]. This is a higher binding energy than metallic Ni [19], which, together with the strong satellite at ≈862 eV, indicates that the nickel is oxidized. Earlier DFT calculations predicted that incorporated Ni atoms are Ni(II) [11], as in $NiFe_2O_4$.

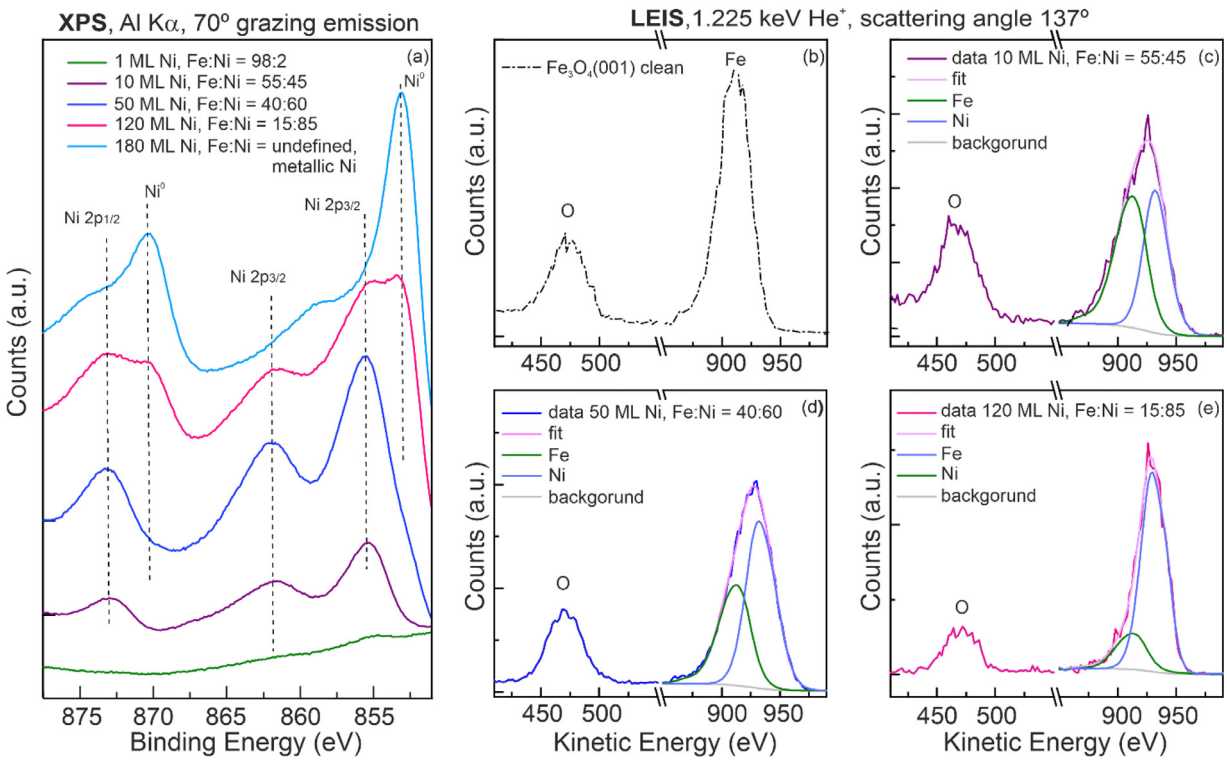

Fig. 2. XPS (Al Kα, 70° grazing emission) and LEIS spectra (1.225 keV He^+, scattering angle 137°). (a) XPS spectra of the Ni 2p region after doping the Fe_3O_4(001-$\sqrt{2} \times \sqrt{2}$)R45° surface with 1 ML Ni (green), 10 ML Ni (purple), 50 ML Ni (blue), 120 ML Ni (pink), and 180 ML Ni (light blue). XPS spectra of the corresponding Fe 2p region can be found in Figure S 1a in the supporting information. (b-e) LEIS spectra of the clean and Ni-doped Fe_3O_4(001)-($\sqrt{2} \times \sqrt{2}$)R45° surfaces shown in (a), and corresponding fits. The fitted spectra show an Fe:Ni ratio of (c) 55:45, (d) 40:60, and (e) 15:85, for the 10 ML Ni-, 50 ML Ni-, and 120 ML Ni-doped magnetite surface respectively. The LEIS spectra shown are the result of averaging of several consecutive scans and their fits were obtained using the software CasaXPS.

As the Ni deposition increases to 10 ML, the Ni $2p_{3/2}$ at 855.5 eV increases in intensity, together with the 861.9 eV satellite and the $2p_{1/2}$ peak at 873 eV, which are harder to see at lower Ni coverage. These features increase in intensity as the Ni deposition increases up to 50 ML. At even higher Ni load (120 ML), two new signals at 853.1 eV and 870.2 eV emerge, indicating that metallic Ni is present on the surface [19]. At 180 ML Ni doping, the XPS spectrum changes shape to a peak with only two main features at 853.1 eV and 870.2 eV, indicating that the surface is fully covered with metallic Ni.

We imaged the Fe_3O_4(001) surface before and after Ni-doping using ambient AFM right after removing the crystal from the UHV chamber (Fig. 3a-d). The corresponding LEED patterns acquired in UHV are shown as insets in each AFM image.

The clean Fe_3O_4(001) surface appears overall flat in ambient AFM, with micrometer-wide terraces separated by step bunches [20] (Fig. 3a). The corresponding LEED pattern exhibits the ($\sqrt{2} \times \sqrt{2}$)R45° periodicity of the SCV reconstruction [10] (yellow square in the inset).

Fig. 3b shows the AFM image of a magnetite surface doped with 50 ML Ni. The large terraces as well as the step bunches observed earlier [20] on the clean magnetite remain visible, suggesting that the doping did not affect the overall surface morphology. Isolated (white) features 0.4-0.6 nm high are visible on the surface. Based on the corresponding line profile (Fig. 3a´; blue), which shows step heights similar to what is observed in Fig. 3a, we suspect these to be residues originating from dust or carbonaceous species. The LEED pattern in the inset shows that the reconstruction spots are now absent and a (1 × 1) symmetry is observed (blue square), which is known to occur above 1 ML Ni atoms incorporated in the subsurface [11].

Fig. 3c-d show AFM images of magnetite surfaces following doping with 120 ML and 180 ML Ni, respectively. The surface in (c) exhibits a rougher morphology than observed in (a) and (b), with a corrugation of ≈0.5 nm (Fig. 3c´; lilac). Accordingly, the corresponding LEED pattern shows weaker (1 × 1) spots. Following higher Ni doping, the surface morphology changes considerably (d). Although the step bunches are still visible underneath, the surface appears covered in round features having height of ~2nm (Fig. 3d´; lilac). Based on the XPS data showed in Fig. 2a, we assign these features to metallic Ni clusters. The corresponding LEED pattern shows very weak (1 × 1) spots with a high background, indicating an increasing fraction of the surface covered by structures with no well-defined crystallographic relationship to the substrate, in agreement with the presence of metallic agglomerates on the surface.

A quantitative measurement of the surface composition, given as the Fe:Ni ratio for each Ni modified surface can be obtained with LEIS measurements (Fig. 2b-e). The clean surface exhibits a LEIS peak centered at 910 eV (Fig. 2b), corresponding to the surface Fe atoms. Following 10 ML Ni doping, the LEIS signal is broader and shifts to higher kinetic energy KE (Fig. 2c, purple). This peak can be well fitted by a (slightly shifted) peak from the surface Fe and an additional component at 931 eV corresponding to the Ni (Fig. 2c, green and blue respectively). By comparing the area of the Fe and Ni contributions we can estimate an Fe:Ni top surface ratio on the 10 ML Ni-doped surface of 55:45. Similarly, we calculate that the surfaces following 50 ML and 120 ML Ni-doping show Fe:Ni ratios of 40:60 and 15:85, respectively. At higher Ni-doping (180 ML) the whole surface is covered in metallic Ni particles, which makes it difficult to use LEIS to quantify the Fe:Ni surface ratio. Therefore, we restrict ourselves to the coverage regime prior to the formation of metallic Ni clusters.

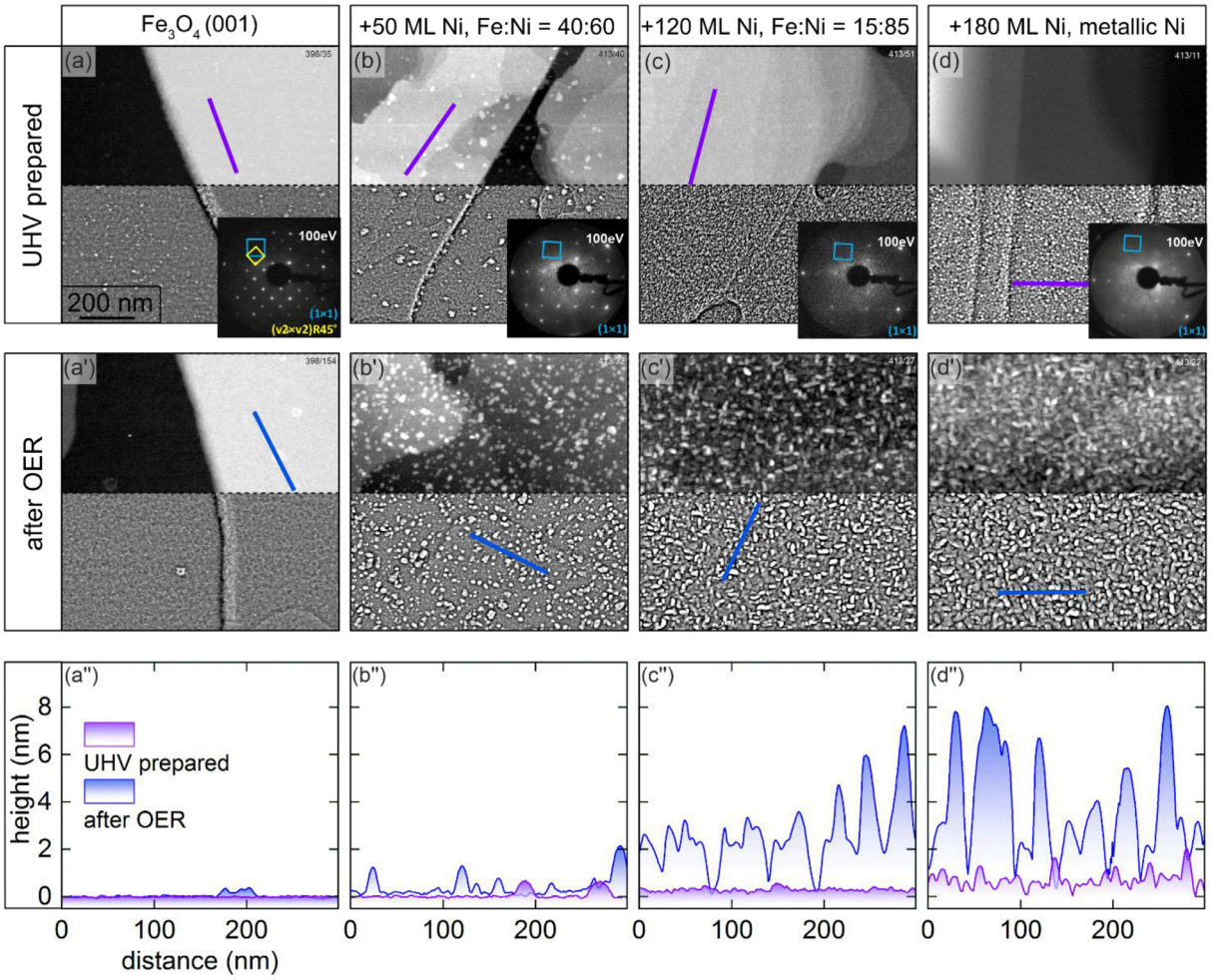

Fig. 3. Ambient-AFM images of the clean and Ni-doped Fe_3O_4(001) surfaces before and after OER in 1 M NaOH. The surface morphologies of the (a) clean Fe_3O_4(001), and Ni-doped surfaces following (b) 50 ML Ni, (c) 120 ML Ni, and (d) 180 ML Ni deposition before OER are shown together with the corresponding LEED pattern acquired in UHV (insets). The middle part of the figure (a-d) shows the morphology of the above-mentioned surfaces after they have been exposed to the electrolyte for three days and cycled until a stable OER current was observed. Each AFM image is shown without (top half) and with (bottom half) high-pass filter. The bottom part of the figure, (a´-d´), shows the corresponding line profiles of the surfaces as prepared in UHV (lilac) and after OER (blue).

Fig. 2b-e also shows how the surface oxygen peak (centered at ~470 eV) evolves as a function of the Ni doping. The intensity of the surface oxygen peak seems to remain constant as the Fe:Ni ratio decreases down to 40:60. Differently, a clear decrease in the oxygen intensity is observed for the surface with lower Fe:Ni ratio (15:85). We can speculate that this behavior correlates with the presence of some metallic Ni on top, as observed in the XPS in Fig. 2a, pink.

Importantly, no systematic change in consecutive scans was observed, which rules out substantial damage to the surface by He^+ sputtering during LEIS measurements. In what follows, we will use the LEIS-determined Fe:Ni ratio to refer to our model catalysts.

3.2. Electrochemical performance

The electrochemical performance of the clean and Ni-doped Fe_3O_4(001) surfaces was investigated using cyclic voltammetry. The overpotential required to reach a given current density is a key catalytic parameter to compare several catalysts and to estimate the energetic efficiency of integrated (photo-) electrochemical water splitting devices [3]. The cyclic voltammograms (Fig. 4a) were acquired in 1 M NaOH under Ar with a scan rate of 10 mV s^{-1} after cycling the electrode until a stable OER current could be observed on two subsequent CVs. Data corresponding to the surfaces imaged in Fig. 3a-d are shown, as well as for surfaces with an Fe:Ni ratio of 98:2 and 55:45. Furthermore, CVs collected before and after electrochemical impedance spectroscopy (EIS) measurements - described later in section 3.4 - up to 1mA·cm^{-2} (see Figure S2) showed that our catalysts are stable over the time range of our experiments (typically 5-9 hours).

The clean Fe_3O_4(001) surface shows an overpotential of 597 mV at a current density of 5 mA·cm^{-2} (Fig. 4a, black), and the surface with an Fe:Ni ratio of 98:2 (green) exhibits similar performance. As the Ni content in the subsurface increases, higher activity towards OER is observed. The OER overpotential decreases by ~110 mV when the Fe:Ni ratio is 55:45 (purple), and reaches ~340 mV vs RHE when the Fe:Ni ratio is 40:60. A higher Ni load (Fe:Ni = 15:85, pink) results in a similar activity as the surface with Fe:Ni ratio of 40:60. Additionally, the surface with an Fe:Ni ratio of 15:85 exhibits a pair of anodic and cathodic peaks at 1.369 and 1.311 V *vs* RHE respectively (pink, inset in Fig. 4a), consistent with the reversible oxidation of Ni(II) to a higher oxidation state (III), as it is reported for the case of the nickel hydroxide/oxyhydroxide couple ($Ni(OH)_2$/NiOOH) [21]. It can also be observed that the charge (peak area) of this peak increases with cycling, indicating the growth of a thicker Ni oxide film on top of the Fe_3O_4(001) surface. These observations suggest a change in the Fe:Ni ratio at the surface following electrode cycling. When only metallic Ni is

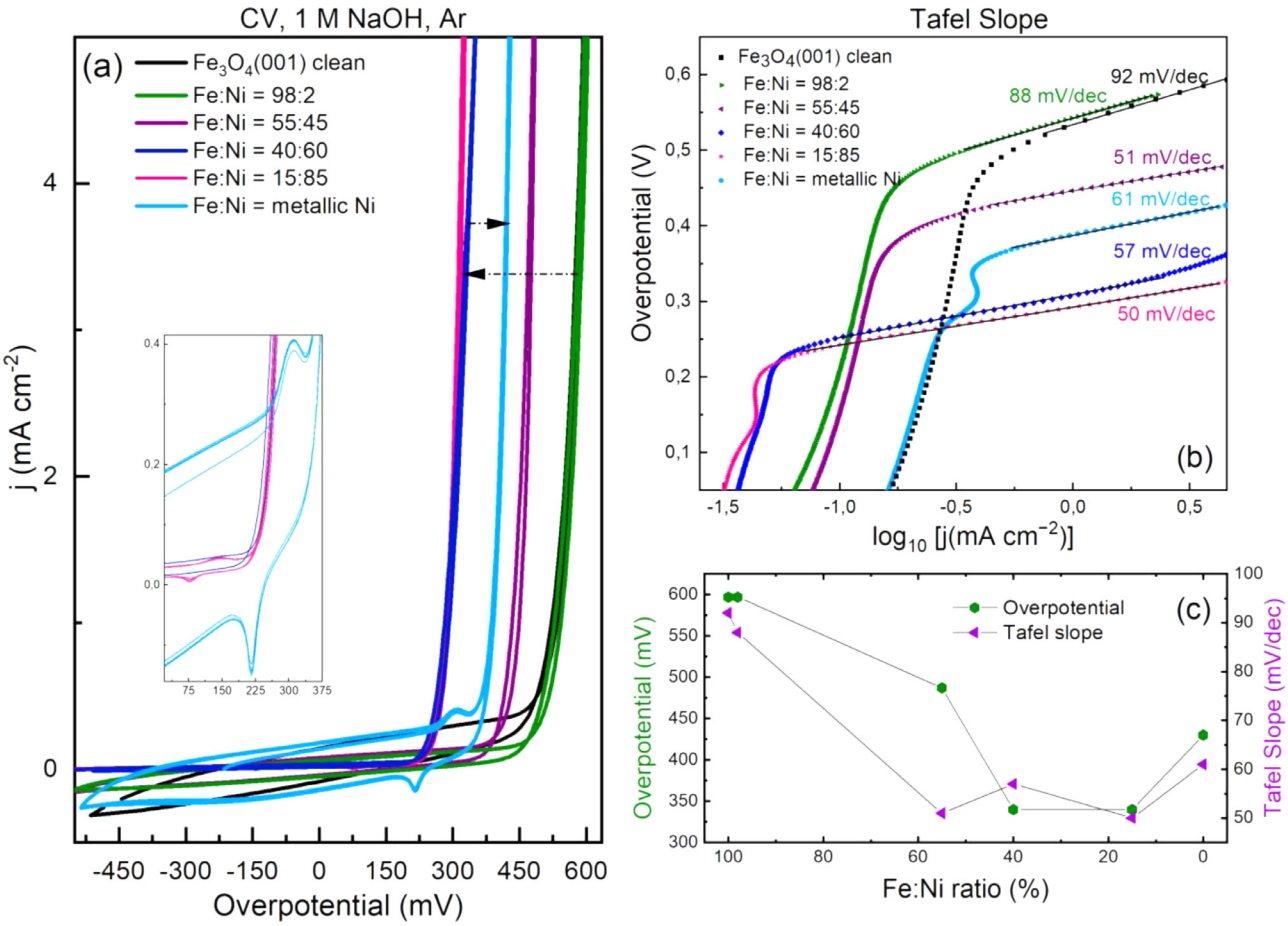

Fig. 4. Oxygen evolution reaction (OER) on clean and Ni-doped $Fe_3O_4(001)$ surfaces. (a) Cyclic voltammetry acquired in 1M NaOH, Ar atmosphere, and with a 10 mV/s scan speed. (b) Tafel slopes obtained from data in (a). In these panels the clean $Fe_3O_4(001)$ is plotted in black, and the Ni-doped surfaces with an Fe:Ni LEIS (surface composition) ratio of 98:2, 55:45, 40:60, 15:85, and the one covered in metallic Ni are reported in green, purple, blue, pink, and light blue, respectively. The corresponding fit of the overpotential curve used for calculating the Tafel slopes is shown as black line for each curve and the length of each black line indicates the region used for the fit. (c) Overpotential for j = 5 mA·cm^{-2} (left axis) and Tafel slopes (right axis) values from (a) and (b) as a function of the surface Fe:Ni ratio (expressed in percent). This diagram shows that the lowest overpotential is obtained for an ideal surface Fe:Ni ratio between 15-40% range.

present on the as-prepared sample, an increase in the overpotential of ~88 mV is observed (Fig. 4a, light blue). A corresponding increase in the charge of the $Ni(OH)_2$/NiOOH peak is observed, as well as anodic shifts of 170 mV and 130 mV for the anodic and cathodic peaks respectively. A similar anodic shift of the Ni peak has been observed with increasing Fe:Ni ratio in the NiOOH phase either by co-deposition of Fe during the film synthesis [22,23] or by incorporation of Fe impurities from the electrolyte into NiOOH electrodes [24]. Moreover, the charge of the $Ni(OH)_2$/NiOOH peak remains constant with cycling, indicating a saturation of the surface with nickel (oxy)hydroxide.

As a comparative metric of activity, Tafel plots are also shown (Fig. 4b). The determination of Tafel slopes can help elucidating the rate-limiting step of a mechanism, but their analysis is particularly difficult in the case of multiple electron-proton transfer reactions such as OER [3]. The clean and low Ni-doped (Fe:Ni = 98:2) surfaces display values of 92 mV/dec and 88 mV/dec respectively, whereas the Ni-doped $Fe_3O_4(001)$ surfaces with a Ni load of 50-85% all show similar values in the range 50-61 mV/dec.

In Fig. 4c we plot the overpotential values and the Tafel slopes showed in Fig. 4a-b as a function of the surface Fe:Ni ratios. Interestingly, the lowest OER overpotential values are obtained for the catalysts with a surface Fe:Ni ratio between 15-40 %, in agreement with what is reported in literature for the best OER powder catalysts [9]. Furthermore, the Tafel slopes fall in the same range as observed for NiFe (oxy)hydroxide catalysts, which typically vary between 25 and 60 mV/dec [9], which could point towards a similar OER reaction mechanism [21].

To check whether catalyst aging in electrolyte affects the activity, we performed cyclic voltammetry on the same surfaces after leaving the Ni-doped electrodes for three days in electrolyte. Fig. 5a-b show CVs of the surfaces with an Fe:Ni ratio of 40:60 (blue), 15:85 (pink), and a sample with metallic Ni clusters (light blue); the dashed curves show the performance after aging. The aged samples show a decrease of the OER overpotential by ~20-100 mV, in good agreement with what has been observed for powder catalysts prepared by wet chemistry [9,25]. Interestingly, the surface with an Fe:Ni ratio of 15:85 is similarly active to the one with Fe:Ni ratio of 40:60 when freshly prepared, but shows a much lower onset of the overpotential after aging. This observation indicates a profound structural difference in the two catalysts, despite the similar performance at first. Fig. 5b shows a magnification of the capacitive regions of the CVs. The Ni-doped magnetite with metallic Ni at the surface (light blue) shows an anodic oxidation peak before OER onset and subsequent cathodic reduction in the backward scan direction. On the surface with an Fe:Ni ratio of 15:85 (pink), these peaks evolve upon cycling and aging, both in terms of charge as well as shift in overpotential. However, this effect is not so marked in the case where the whole surface is covered with metallic Ni clusters, where only a (slight) shift in poten-

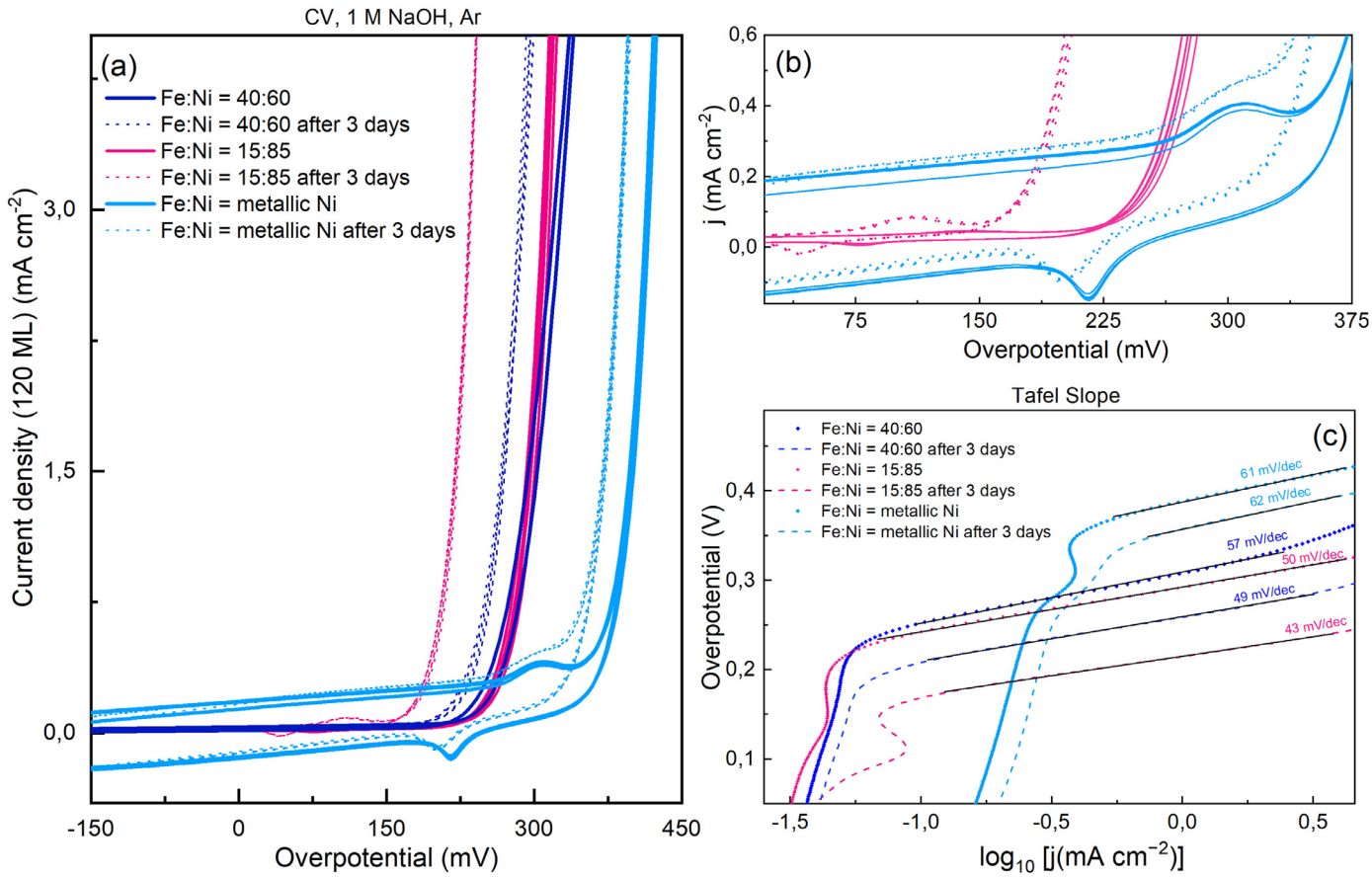

Fig. 5. Oxygen evolution reaction (OER) on clean and Ni-doped $Fe_3O_4(001)$ surfaces before and after three days aging. (a) Cyclic voltammetry acquired in 1M NaOH, under Ar atmosphere, and with a 10 mV·s^{-1} scan rate. (b) Zoom into the lower overpotential region shows changes in the anodic and cathodic waves for the surfaces with higher Ni load, before the OER onset. (c) Tafel plots obtained from data in (a) with Tafel slopes indicated. Each panel shows the activity of the Ni-doped surfaces with an Fe:Ni ratio of 40:60, 15:85, and the one with metallic Ni clusters, right after preparation (solid blue, pink and light blue), and after aging the sample in electrolyte for three days (dashed blue, pink and light blue). The corresponding fit of the overpotential curve used for calculating the Tafel slopes is shown as black line for each curve and the length of each black line indicating the region used for the fit.

tial is observed (blue). The interpretation of the redox behavior is in general very difficult due to possible formation of electrically disconnected domains upon cycling because of the different conductivity of the oxidized and reduced phase [26].

Fig. 5c shows the comparison of the Tafel plots for the surfaces in (a). The aged surfaces show Tafel slopes values in the range 43-62 mV/dec range, similarly to the freshly prepared catalysts (Fig. 4b).

3.3. Catalyst surface characterization after reaction

Fig. 3a´-d´ shows the AFM characterization of the surfaces imaged in Fig. 3a-d after OER and three days aging in electrolyte. Before imaging, each surface was rinsed in milli-Q water several times, for several minutes and blow-dried using a gentle Ar flow to minimize the presence of salt residue from the electrolyte.

The morphology of the clean $Fe_3O_4(001)$ remains unchanged after OER (a´), and shows a smooth appearance with the wide terraces and step bunches still visible, in agreement with earlier stability tests[20]. The presence of small particles (white) is associated with residue from the electrolyte.

Fig. 3b´ shows the AFM image of the surface imaged with initially 40:60 Fe:Ni (Fig. 3b) after resting in electrolyte for three days, followed by cycling the electrode until a stable current was observed (Fig. 5). The terraces and step bunches remain visible underneath, but white features of irregular shape and height between 1-2 nm are now common on the surface (blue line profile in Fig. 3b´).

Fig. 3c´-d´ show AFM images of the 15:85 and metallic Ni surfaces, respectively, after the electrode has been exposed to the electrolyte for three days and cycled until a stable OER current was observed (Fig. 5). Their morphologies appear similar in AFM. Due to the appearance of protrusions with 3-7 nm (line profile in Figure 3 c´; blue) and 4-8 nm high (line profile in panel d´; blue), it is almost impossible to discern remainders of the original surface morphology consisting of flat and wide terraces. Since the density and height of the protrusions increases with Ni content, they likely consist of a Ni-(oxy)-hydroxide phase, grown from pre-existent metallic Ni upon electrochemical cycling [25], in agreement with equilibrium potential–pH diagrams (i.e. Pourbaix diagrams) that show NiOOH as the predominant species in neutral-to-basic aqueous solutions at OER potentials [25].

3.4. Electrochemical impedance spectroscopy

Electrochemical impedance spectroscopy (EIS) measurements were performed on the Ni-doped model catalysts electrochemically investigated in Fig. 4. In the OER region the EIS Nyquist plots (Figure S3a) exhibit two relaxation processes characterized by two semi-circles that can be assigned to two capacitances while the phase in Bode plots (Figure S3b) exhibits two maxima eventually merging into a broad peak. This impedance behavior is consistent with previous measurements on metal transition oxides and per-

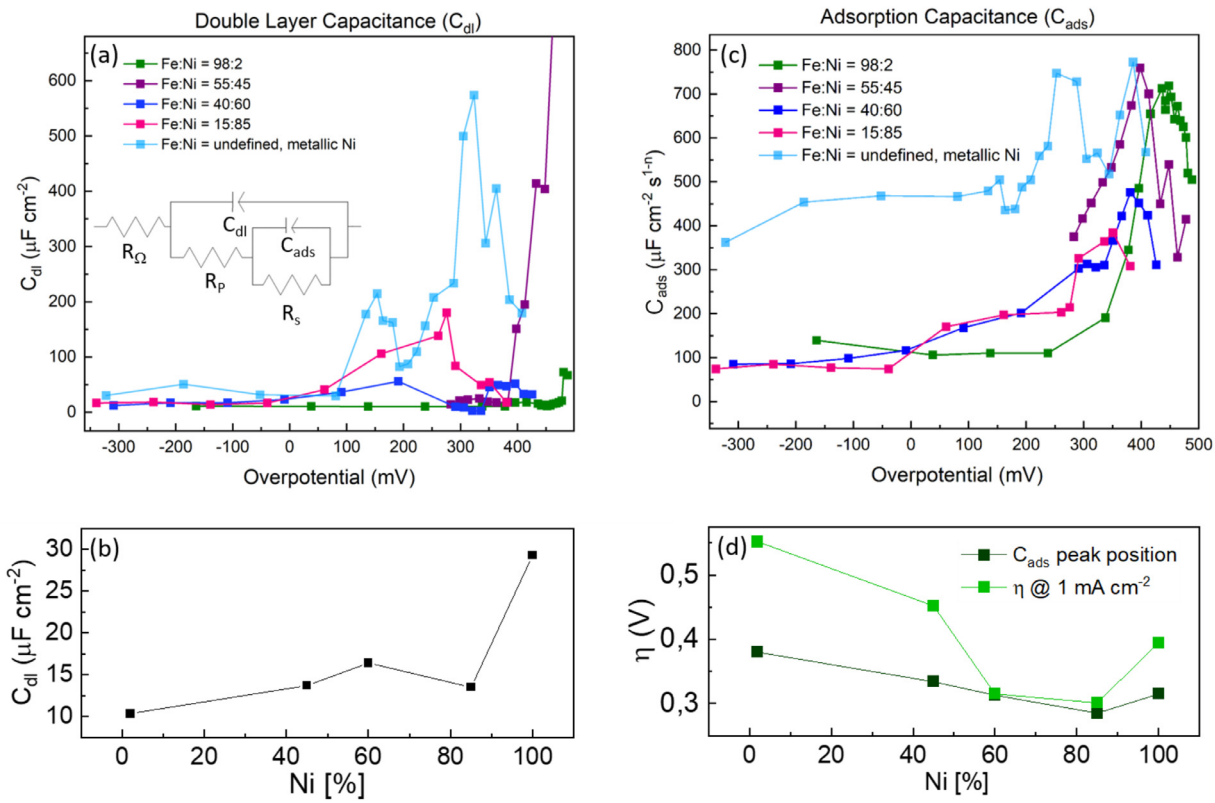

Fig. 6. Electrochemical impedance spectroscopy on Ni-doped Fe_3O_4(001) surfaces. (a) Double layer capacitance and (b) minimum values of C_{dl} in the double-layer region;(c) adsorption capacitance (C_{ads}) and potential of the maximum of C_{ads} for the Ni-doped magnetite surfaces. In panel (a) and (c) capacitance values are shown for the Ni-doped Fe_3O_4(001) surfaces with an Fe:Ni ratio of 98:2, 55:45, 40:60, 15:85, and the one fully covered in metallic Ni clusters are reported in green, purple, blue, pink, and light blue, respectively. The equivalent circuit used to fit the electrochemical impedance spectroscopy data is shown as an inset in (a) and it consists of the following elements: R_Ω represents the uncompensated solution resistance; C_{dl} models the double layer capacitance; the polarization resistances R_P in combination with R_S are commonly interpreted as the charge transfer resistances of the electrosorption and desorption processes. Finally, $C_{ads,}$ the adsorption pseudo-capacitance in parallel with R_S models the relaxation of the charge associated with the adsorbed intermediate [27].

ovskites during the OER. [27,28,29] The EIS response can be modelled by the equivalent circuit (EC) shown as an inset in Fig. 6a with a double-layer capacitance (C_{dl}) in parallel with the combination of a polarization resistance (R_p) and an adsorption pseudo-capacitance (C_{ads}) in parallel with a resistor R_s. The C_{dl} element accounts for the charging of the electrified interface. C_{ads} models the accumulation of an adsorbed intermediate involved in the rate-limiting step of the OER. The sum of the resistive elements R_s and R_p bear a physical meaning as the zero-frequency electron transfer resistance defined as $R_f = R_p + R_s$, i.e., the slope of the steady-state polarization curve after Ohmic-drop compensation. R_Ω represents the electrolyte resistance. It has to be noted that both capacitors were modeled as constant phase elements (CPEs), defined as $Z = C_{n=1}^{-1}(j\omega)^{-n,}$ where $C_{n=1}^{-1}$ is the impedance of the capacitor without frequency dispersion, i.e., if the coefficient $n = 1$ which is the case for a perfect capacitor. The interpretation of the CPEs dispersion coefficient n is varied and complicated; its origin has been attributed to surface roughness, inhomogeneities, or inhomogeneous adsorption of ions [30]. In the double-layer region, prior to the onset of the OER, we will show in a separate work that the impedance response of the single-crystal magnetite electrode has to be modified by adding a Warburg element in series with C_{ads} corresponding to a diffusion impedance that we attribute to electrolyte cations intercalating into the oxide (Figure S4a). Of interest in this work is the impedance response in the OER region.

All the surfaces investigated in this work, with the exception of the one fully covered by metallic Ni clusters (light blue), show a roughly constant double layer capacitance values in the 10-25 μF·cm^{-2} range prior to the OER onset (Fig. 6a). The exponent of the CPE element used for the fitting was equal to 1 in the double-layer region (Figure S4d) and diverged from 1 at high current densities or when Ni is exposed such that $Ni(OH)_2$ is oxidized to NiOOH. These values are comparable to a C_{dl} observed on metallic single crystals, suggesting that our catalysts have a perfect capacitor-like behavior. Fig. 6c shows the value of this capacitance as a function of the Ni content: C_{dl} slightly increases from 10 to 15 μF cm^{-2} as the Ni loading increases, but a higher value is observed in the case of the surface fully covered with Ni metallic clusters (180 ML). The higher C_{dl} values observed for this surface may be explained by the formation of an irregular $Ni(OH)_2$ layer upon oxidation of the metallic Ni by contact with the electrolyte. In this way, more active surface area is exposed to the electrolyte and polarized, leading to a higher C_{dl}.

The adsorption capacitance plot in Fig. 6c shows that the Ni-doped Fe_3O_4(001) surfaces display a peak with similar C_{ads} values independent of the Ni doping level, which however shifts to lower overpotential as the Ni load increases (Fig. 6d). The surface fully covered with metallic Ni clusters appears to develop two additional capacitance peaks (Fig. 6c). The overlay of the corresponding CV and C_{ads} in Figure S3e, shows that the additional initial (pre-)peak is observed at the same potential as the $Ni(OH)_2$ oxidation peak.

The group of Bandarenka [31,32] associated the observation of peaks or increase in C_{ads} to the adsorption of OER reaction intermediates and reported them for various transition metal oxides. These observations suggest that the formation of the intermediate species before the onset of the OER involves similar mechanisms for pure and Ni-modified magnetite. This is also supported by the

fact that value of C_{ads} retains similar values at the maximum of the peak. From the capacitance data in Fig. 6a and c we can draw the following conclusions: (i) given that the initial C_{dl} values hardly vary with Ni loading, there is no significant increase in electrochemically active surface area, and the catalytic effect of Ni shown in Fig. 4 cannot be ascribed to an effective enhancement of the surface area; (ii) the fact that a similar peak in C_{ads} is observed for all surfaces, also the one where Fe is expected to be the only active site (98:2), would be in agreement with the commonly held view that Fe is the active site in NiFe catalysts, but that it becomes more active in an Ni environment. The presence of two peaks in the EIS of the metallic Ni-decorated surface if not a noise effect can be interpreted as two types of adsorbates on Ni (and perhaps Fe) sites that are accessible due to the porosity and layered structure of Ni films, providing access to active sites down to 5 nm in depth [33].

4. Discussion

The experimental data acquired on clean and Ni-doped $Fe_3O_4(001)$ surfaces show that Ni doping enhances the OER activity of magnetite. Electrochemical voltammetric responses, in combination with surface sensitive techniques, suggest a strong dependence of the OER activity on the atomic structure of the surface exposed to electrolyte. In particular, LEIS measurements indicate that the catalyst with the best OER performances, with an overpotential of 340 mV vs RHE at 5 mA·cm^{-2}, exhibits a surface Fe:Ni ratio of 40:60.

In order to shed light on how the presence of Ni affects the magnetite atomic surface structure-activity relationship, the following observations have to be considered:

We have previously shown that following 1 ML Ni-doping and subsequent mild annealing at 200°C, the Ni atoms fill all the vacant sites in the $Fe_3O_4(001)$ subsurface, resulting in neighboring Fe and Ni in the second surface layer [8]. The voltammetric response of this surface (green, Fig. 4a) shows no improvement in the OER activity compared to the clean magnetite. Corresponding LEIS measurements (see supplemental material, Figure S6) suggest that this surface exhibits a surface Fe:Ni ratio of 98:2, confirming that almost no Ni is present in the outermost surface layer. These results suggest that the presence of subsurface Ni is insufficient to improve the OER activity. Based on our XPS and LEED data, we propose that modification of the $Fe_3O_4(001)$ surface with a Ni load > 1 ML leads to the formation of a multilayer mixed ferrite spinel oxide with a structure similar to $Ni_xFe_{3-x}O_4$-like systems. Now the model catalyst exposes both, Fe and Ni atoms in the outermost surface layer as seen from LEIS. In these conditions, the OER activity increases, reaching a maximum when the surface exposes an optimum Ni content of 60-85%. XPS and LEED suggest that the structure of this surface stays characteristic of mixed spinel up to a Ni doping corresponding to a surface Fe:Ni ratio of 40:60. Higher Ni doping results in the formation of metallic Ni clusters, which compromise the spinel long-range order, leading to a loss of atomic control without substantial further enhancement of the activity and, eventually, a decrease in the OER activity when Fe is no longer accessible.

Our AFM results suggest that the surface prepared with an Fe:Ni ratio of 40:60 appears stable after OER, albeit with some new features, 1-2 nm high, scattered all over the surface. In contrast, the surfaces with higher Ni loads show the growth of a new phase, which increases in volume and roughness (effective surface area) as the metallic Ni concentration increases. This suggests the growth of a new phase on top of the doped magnetite surface. On the basis of our XPS results, as well as earlier studies [25,34,35], we interpret this phase as the growth of Ni-(oxy)-hydroxide. Similar phases have been also observed on powder Fe-Ni based catalysts, and have reported in literature to affect the catalytic activity towards OER [9]. In particular, Burke *et al.* [25] observed that electrochemical cycling leads to a transformation from nanocrystalline NiO_x films to a layered (oxy)-hydroxide that correlates with an increase in OER activity. Similarly, Deng *et al.* [35] monitored the dynamic changes of single layered $Ni(OH)_2$ using *in situ* electrochemical-AFM, and observed dramatic morphology changes already after one linear voltammetry sweep, as well as a direct relation between increase in OER activity and increase in volume and redox capacity of the layered oxy-hydroxide phase. Our results are, however, are not entirely in agreement with these observations. The increase in volume and surface area of the hydroxide phase does not correlate directly with our catalysts' activity: the surface with the highest amount of the Ni-(oxy)-hydroxide phase and redox capacity is ≈ 200 mV less active than the (almost) flat surface with Fe:Ni ratio 40:60. At this Ni surface concentration, we do not observe in AFM (Figure 3b́) the growth of the new phase covering a large fraction of the surface, but only some scattered features. Nevertheless, the activity of this surface (expressed by the overpotential, Fig. 5a) is close to the optimum. This clearly indicates that the layered Ni-(oxy)-hydroxide is not the active phase in our catalyst.

It is also important to mention that the activity exhibited by the surface prepared with a Fe:Ni ratio of 40:60, with an overpotential of 340 mV vs RHE is comparable to values reported for OER on (Fe)Ni based catalysts [34-40]. For comparison, the overview in Table 1 shows a selection of some of the best OER catalysts based on Ni-Fe oxides reported in literature. The lowest overpotential values measured on these catalysts at 5 mA·cm^{-2} vary typically in the 210 - 347 mV vs RHE range (in 1 M KOH or NaOH electrolyte). Similar overpotential values were also obtained from our surface prepared with a higher Ni load (Fe:Ni = 15:85).

When comparing the latter surface with the one having an Fe:Ni ratio of 40:60 after electrochemical cycling and subsequent aging for three days in electrolyte, a different activity trend is observed (dashed lines in Fig. 5a). On the one hand, both surfaces show a significant increase in activity following voltammetric cycling and aging, in agreement with previous studies [3,35]. On the other hand, their activity does not increase in the same way. Surprisingly, the surface with metallic Ni shows a much lower onset of the OER overpotential than the one with an Fe:Ni of 40:60, despite the similar performances when freshly prepared. This surface is by far the most active with an overpotential of 247 mV vs RHE. However, it has to be taken into account that this surface, being characterized by the presence of a large fraction of metallic Ni in the as-prepared state, shows neither a well-defined spinel structure nor any other ordered structure over most of the surface and, therefore, cannot serve as a model system. Since one of the scopes of this work is to propose a working model system for the understanding of the OER mechanism, a compromise between activity and the ability to preserve atomic control has to be made. In this regard, the surface with a Fe:Ni ratio of 40:60, very well defined, stable and highly active, fits the criteria to be used as model catalyst.

Finally, the analysis of the Tafel plots and adsorption capacitance measurements can help extracting information to identify the OER active sites. Our Ni-modified magnetite surfaces show similar absolute Tafel slopes values (Figs. 5b and 6c) in the 43-62 mV/dec range, independent of the degree of Ni doping for Fe:Ni ratios down to 15:85. Furthermore, the clean and the Ni-modified surfaces show similar maximum values of the adsorption capacitance before the OER onset. These values are associated to the appearance of the OER precursors [31,32] and the shift to lower overpotentials as the Ni doping increases and finally reaches a steady value with the optimal Ni content (Ni content ≈ 60-80%).

To explain these observations, we propose the following scenario: the intermediate species that forms on the surface before

Table 1
Comparison of our model system activity with real catalysts from recent works.

Catalyst	Ni:Fe ratio	Electrolyte	Overpotential vs RHE (mV) at $j = 5\ mA{\cdot}cm^{-2}$	Tafel Slope ($mV{\cdot}dec^{-1}$)	Ref. (year)
Ni-Fe_3O_4(001)	60:40	1 M NaOH	340	57	This work
$NiFeO_x$ film	9:1	1 M KOH	336	30	Ref.[36] (2013)
NiFe LDH	3:1	1 M KOH	347	67	Ref.[37] (2014)
NiFe LDH	80:20	1 M NaOH	260	21	Ref.[38] (2016)
Ni-Fe	4:1	1 M KOH	331	58	Ref.[39] (2015)
NiFe LDH	78:22	1 M KOH	280	47.6	Ref.[40] (2014)
NiFe LDH/CNT	5:1	1 M KOH	247	31	Ref.[41] (2013)
NiFe/NF	3:1	1 M KOH	215	28	Ref.[42] (2015)

Abbreviations: LDH, layered double hydroxide; NF, Ni foam; CNT, carbon nanotubes.

the onset of the OER might be the same on the clean surface as well as on the Ni- modified one, indicating Fe as the active sites. Accordingly, the right amount of Ni in the spinel surface does not cause the formation of intermediates but facilitates it. Similar conclusions have been proposed by Bell and co-workers who used DFT to compare the OER activity of pure and Fe-doped γ-NiOOH and of pure and Ni-doped γ-FeOOH catalysts [43]. They showed that pure γ-NiOOH adsorbs the OER intermediates too weakly and pure γ-FeOOH too strongly. They found a considerable increase in activity for Fe sites that are surrounded by Ni next-nearest neighbours in both γ-NiOOH and γ-FeOOH. Similar results have also been obtained by Klaus et al. who, on the basis of turnover frequency (TOF) calculations, proposed Fe atoms as the OER active sites in Fe-doped NiOOH catalysts [24].

Nevertheless, despite the fact that the OER mechanism on NiFe-based catalysts is still unclear together with several fundamental open questions such as the clear identification of the rate limiting step, our results tend to confirm that the OER intermediates are located on Fe sites, the surrounding Ni having a promoting effect on the latter. Furthermore, a deep understanding of the observed electrode aging effect on the OER activity, following long exposure of the material to the electrolyte, remains open, but reveals the importance of the nature of the electrolyte and its interaction with the material.

Moreover, it should be pointed out that the use of a single crystal enables an accurate determination of the electrochemically active surface area (ECSA) of these materials and provides reference values for the double-layer capacitance and adsorption capacitance on Fe-Ni based catalysts. The double-layer capacitance values are slightly affected by the Fe:Ni ratio and this should be taken into consideration for further determination of the ECSA of such electrodes [31,32]. Additionally, our results point out that, beyond the Fe:Ni ratio, the nature of the interface (spinel or separated NiOOH/Fe-Ni spinel) significantly affects the capacitance of the interface and its use as a reference for ECSA determination could be compromised.

5. Conclusions

The high intrinsic OER activity of mixed Fe-Ni oxides motivated our efforts to make further steps in the understanding of the fundamental roles of Fe and Ni in OER catalysis.

In this work, we show a combined surface science/electrochemistry approach for the preparation of well-defined Ni-modified Fe_3O_4(001) surfaces and the investigation of their electrochemical performances with respect to OER. We have found that the surface prepared with an Fe:Ni ratio of 40:60 shows a performance comparable to those of the best powder catalysts reported in literature, and still maintains a well-defined structure. Being at the same time simple, highly active, and stable under operation conditions, this surface is an ideal candidate to serve as a working model system to gain atomic-scale insights into the complicated OER mechanism. Whereas a Ni-based phase, probably a Ni (oxy)hydroxide covers all of the surface at high Ni coverage, the highest activity is observed when the Ni-modified Fe_3O_4(001) surface is still accessible, indicating that this surface is essential for the reaction. Electrochemical impedance spectroscopy suggests that on our Fe-Ni catalyst, the active site for the OER is located on Fe atoms at the surface regardless of the Ni:Fe ratio in the structure, suggesting that the Ni does not cause the formation of intermediates but facilitates it.

Putting our results in the context of future perspective, a well-defined model system such as the Ni-modified Fe_3O_4(001) presented in this work is desirable to address the fundamental aspects that are still controversial. With a limited variety of possible adsorption sites and being accessible to methods benefitting from on single-crystal surfaces, this model surface could thus be used for further investigations on the exact nature of the adsorbates involved in the rate limiting step, using *in-situ* surface science techniques, to shed more light on key parameters to improve the stability and activity of amorphous catalysts used in water splitting devices. We also believe that the good agreement of our results with what is reported in the literature for powder or amorphous catalyst makes our model surface worthwhile to be used as a model to guide future computational studies.

Credit author statement

Francesca Mirabella: Conceptualization, Methodology, Data Curation, Writing- Original draft preparation; Matthias Müllner: Conceptualization, Methodology, Data Curation; Thomas Touzalin: Conceptualization, Methodology, Data Curation; Michele Riva: Reviewing and Editing; Zdenek Jakub: Reviewing and Editing; Florian Kraushofer: Reviewing and Editing; Michael Schmid: Reviewing and Editing; Marc T.M. Koper: Supervision, Reviewing and Editing; Gareth S. Parkinson: Supervision, Reviewing and Editing, Ulrike Diebold: Supervision, Reviewing and Editing.

Declaration of Competing Interest

None.

Acknowledgments

This work was supported by the European Union under the A-LEAF project (732840-A-LEAF), by the Austrian Science Fund FWF (Project 'Wittgenstein Prize, Z250-N27), and by the European Research Council (ERC) under the European Union's HORIZON2020 Research and Innovation program (ERC Grant Agreement No. [864628]).

Supplementary materials

Supplementary material associated with this article can be found, in the online version, at doi:10.1016/j.electacta.2021.138638.

References

[1] G. Centi, S. Perathoner, R. Passalacqua, C. Ampelli, in: Carbon Neutral Fuels and Energy carriers, 4, CRC Press, 2011, p. 291. Chapter.

[2] T.A. Faunce, L. Wolfgang, A.W. Rutherford, D. MacFarlane, G.F. Moore, P. Yang, D.G. Nocera, T.A. Moore, D.H. Gregory, S. Fukuzumi, K.B. Yoon, F.A. Armstrong, M.R. Wasielewskin, S. Styringo, Energy and environment policy case for a global project on artificial photosynthesis, Energy Environ. Sci. 6 (2013) 695.

[3] C.C.L. McCrory, S. Jung, J.C. Peters, T.F Jaramillo, Benchmarking Heterogeneous Electrocatalysts for the Oxygen Evolution Reaction, J. Am. Chem. Soc. 135 (2013) 16977–16987.

[4] W.T. Hong, M. Risch, K.A. Stoerzinger, A. Grimaud, J. Suntivich, Y. Sao-Horn, Toward the rational design of non-precious transition metal oxides for oxygen electrocatalysis, Energy Environ. Sci. 8 (2015) 1404–1427.

[5] E. Fabbri, A. Habereder, K. Waltar, R. Kötz, T.J. Schmidt, Developments and perspectives of oxide-based catalysts for the oxygen evolution reaction, Catal. Sci. Technol. 4 (2014) 3800–3821.

[6] H. Hajiyani, R. Pentcheva, Surface Termination and Composition Control of Activity of the $Co_xNi_{1-x}Fe_2O_4$(001) Surface for Water Oxidation: Insights from DFT+ U Calculations, ACS Catal 8 (2018) 11773–11782.

[7] Z. Wu, Y. Zhao, W. Jin, B. Jia, J. Wang, T Ma, Recent Progress of Vacancy Engineering for Electrochemical Energy Conversion Related Applications, Adv. Funct. Mater. 31 (2021) 1–36.

[8] Z. Wu, D. Nie, M. Song, T. Jiao, G. Fu, X. Liu, Facile synthesis of Co-Fe-B-P nanochains as an efficient bifunctional electrocatalyst for overall water-splitting, Nanoscale 11 (2019) 7506–7512.

[9] F. Dionigi, P. Strasser, NiFe-Based (Oxy)hydroxide Catalysts for Oxygen Evolution Reaction in Non-Acidic Electrolytes, Adv. Energy Mater. 6 (2016) 1600621.

[10] R. Bliem, E. McDermott, P. Ferstl, M. Setvin, O. Gamba, J. Pavelec, M.A. Schneider, M. Schmid, U. Diebold, P. Blaha, L. Hammer, G.S. Parkinson, Subsurface Cation Vacancy Stabilizatin of the Magnetite (001) Surface, Science 346 (2014) 1215–1218.

[11] R. Bliem, J. Pavelec, O. Gamba, E. McDermott, Z. Wang, S. Gerhold, M. Wagner, J. Osiecki, K. Schulte, M. Schmid, P. Blaha, U. Diebold, G.S. Parkinson, Adsorption and incorporation of transition metals at the magnetite Fe_3O_4(001) surface, Phys. Rev. B 92 (2015) 075440.

[12] G.S. Parkinson, N. Mulakaluri, Y. Losovyj, P. Jacobson, R. Pentcheva, U. Diebold, Semiconductor–half metal transition at the Fe_3O_4(001) surface upon hydrogen adsorption, Phys. Rev. B 82 (2010) 125413.

[13] W. Weiss, W. Ranke, Surface chemistry and catalysis on well-defined epitaxial iron-oxide layers, Prog. Surf. Sci. 70 (2002) 1–1512002.

[14] S. Hiura, A. Ikeuchi, S. Shirini, A. Subagyo, K. Sueoka, Effect of adsorbed H atoms on the Fe electronic states of Fe_3O_4(001) film surfaces, Phys. Rev. B. 91 (2015) 205411.

[15] Z. Jakub, J. Hulva, F. Mirabella, F. Kraushofer, M. Meier, R. Bliem, U. Diebold, G.S. Parkinson, Nickel Doping Enhances the Reactivity of Fe_3O_4(001) to Water, J. Phys. Chem. C 123 (2019) 5038–15045.

[16] R. Gargallo-Caballero, L. Martin-Garcia, A. Quesada, C. Granados-Millares, M. Foerster, L. Aballe, R. Bliem, G.S. Parkinson, P. Blaha, J.F. Marco, J. de la Figuera, Co on Fe_3O_4(001): Towards precise control of surface properties, J. Chem. Phys. 144 (2016) 094704.

[17] G. Zhang, Y. Li, Y. Zhou, F. Yang, NiFe Layered-Double-Hydroxide-Derived NiO-$NiFe_2O_4$ /Reduced Graphene Oxide Architectures for Enhanced Electrocatalysis of Alkaline Water Splitting, ChemElectroChem 3 (2016) 1927–1936.

[18] Z. Wu, Z. Zou, J. Huang, F. Gao, $NiFe_2O_4$ Nanoparticles/NiFe Layered Double-Hydroxide Nanosheet Heterostructure Array for Efficient Overall Water Splitting at Large Current Densities, ACS Appl. Mater. Interfaces 10 (2018) 26283–26292.

[19] A.P. Grosvenor, M.C. Biesinger, R.S.C. Smart, N.S McIntyre, New interpretations of XPS spectra of nickel metal and oxides, Surf. Sci. 600 (2006) 1771–1779.

[20] M. Müllner, M. Riva, F. Kraushofer, M. Schmid, G.S. Parkinson, S.F.L. Mertens, U Diebold, Stability and Catalytic Performance of Reconstructed Fe_3O_4(001) and Fe_3O_4(110) Surfaces During Oxygen Evolution Reaction, J. Phys. Chem. C 123 (13) (2019) 8304–8311.

[21] T. Shinagawa, A.T. Garcia-Esparza, K. Takanabe, Insight on Tafel slopes from a microkinetic analysis of aqueous electrocatalysis for energy conversion, Sci. Rep. 5 (2015) 1–21.

[22] P. Chakthranont, J. Kibsgaard, A. Gallo, J. Park, M. Mitani, D. Sokaras, T. Kroll, R. Sinclair, M.S. Mogensen, T.F. Jaramillo, Effects of Gold Substrates on the Intrinsic and Extrinsic Activity of High-Loading Nickel-Based Oxyhydroxide Oxygen Evolution Catalysts, ACS Catal 7 (2017) 5399–5409.

[23] M.W. Louie, A.T. Bell, An investigation of thin-film Ni-Fe oxide catalysts for the electrochemical evolution of oxygen, J. Am. Chem. Soc. 135 (2013) 12329–12337.

[24] S. Klaus, Y. Cai, M.W. Louie, L. Trotochaud, A.T. Bell, Effects of Fe electrolyte impurities on $Ni(OH)_2$/NiOOH structure and oxygen evolution activity, J. Phys. Chem. C 119 (2015) 7243–7254.

[25] Burke, M. S., Enman, L. J., Batchellor, A. S., Zou, S. & Boettcher, S. W. Oxygen Evolution Reaction Electrocatalysis on Transition Metal Oxides and (Oxy)hydroxides : Activity Trends and Design Principles*Chem. Mater.*27, 22, 7549-7558 (2015).

[26] A.S. Batchellor, S.W. Boettcher, Pulse-Electrodeposited Ni-Fe (Oxy)hydroxide Oxygen Evolution Electrocatalysts with High Geometric and Intrinsic Activities at Large Mass Loadings, ACS Catal 5 (2015) 6680–6689.

[27] M.E.G. Lyons, M.P Brandon, The significance of electrochemical impedance spectra recorded during active oxygen evolution for oxide covered Ni, Co and Fe electrodes in alkaline solution, J. Electroanal. Chem. 631 (2009) 62–70.

[28] R.L. Doyle, M.E.G Lyons, An electrochemical impedance study of the oxygen evolution reaction at hydrous iron oxide in base, Phys. Chem. Chem. Phys. 15 (2013) 5224–5237.

[29] C.S. Hsu, N.T. Suen, Y.Y. Hsu, H.Y. Lin, C.W. Tung, Y.F. Liao, T.C. Chan, H.S. Sheu, S.Y. Chen, H.M. Chen, Valence- and element-dependent water oxidation behaviors: In situ X-ray diffraction, absorption and electrochemical impedance spectroscopies, Phys. Chem. Chem. Phys. 19 (2017) 8681–8693.

[30] R.S. Neves, E. De Robertis, A.J. Motheo, Capacitance dispersion in EIS measurements of halides adsorption on Au (210), Electrochimica Acta 51 (2006) 1215–1224.

[31] S. Watzele, A.S. Bandarenka, Quick Determination of Electroactive Surface Area of Some Oxide Electrode Materials, Electroanalysis 28 (2016) 2394–2399.

[32] S. Watzele, P. Hauenstein, Y. Liang, J. Fichtner, B. Garlyyev, D. Scieszka, F. Claudel, F. Maillard, A.S. Bandarenka, Determination of Electroactive Surface Area of Ni-, Co-, Fe-, and Ir-Based Oxide Electrocatalysts, ACS Catal 9 (2019) 9222–9230.

[33] S. Corby, M.-G. Tecedor, S. Tengeler, C. Steinert, B. Moss, C.A. Mesa, H.F. Heiba, A.A. Wilson, B. Kaiser, W. Jaegermann, L. Francas, S. Gimenez, J.R. Durrant, Separating bulk and surface processes in NiO_x electrocatalysts for water oxidation, Sustain. Energy Fuels 4 (2020) 5024–5030.

[34] F. Kraushofer, F. Mirabella, J. Xu, J. Pavelec, J. Balajka, M. Müllner, N. Resch, Z. Jakub, J. Hulva, M. Meier, M. Schmid, U. Diebold, G. Parkinson, Self-limited Growth of an Oxyhydroxide Phase at the Fe_3O_4(001) Surface in Liquid and Ambient Pressure Water, J. Chem. Phys. 151 (2019) 154702.

[35] J. Deng, M. Nellist, M.B. Stevens, C. Dette, Y. Wang, S.W. Boettcher, Morphology Dynamics of Single-Layered $Ni(OH)_2$/NiOOH Nanosheets and Subsequent Fe Incorporation Studied by in Situ Electrochemical Atomic Force Microscopy, Nano Lett 17 (2017) 6922–6926.

[36] L. Trotochaud, J.K. Ranney, K.N. Williams, S.W. Boettcher, Solution-cast metal oxide thin film electrocatalysts for oxygen evolution, J. Am. Chem. Soc. 134 (2012) 17253–17261.

[37] F. Song, X. Hu, Exfoliation of layered double hydroxides for enhanced oxygen evolution catalysis, Nat. Commun. 5 (2014) 4477.

[38] R. Chen, G. Sun, C. Yang, L. Zhang, J. Miao, H. Tao, H. Yang, J. Chen, P. Chen, B. Liu, Achieving stable and efficient water oxidation by incorporating NiFe layered double hydroxide nanoparticles into aligned carbon nanotubes, Nanoscale Horizons 1 (2016) 156–160.

[39] X. Yu, M. Zhang, W. Yuan, G. Shi, A high-performance three-dimensional Ni-Fe layered double hydroxide/graphene electrode for water oxidation, J. Mater. Chem. A 3 (2015) 6921–6928.

[40] B.M. Hunter, J.D. Blakemore, M. Deimund, H. Gray, Winkler B., R. J., A.M Müller, Highly active mixed-metal nanosheet water oxidation catalysts made by pulsed-laser ablation in liquids, J. Am. Chem. Soc. 136 (2014) 13118–13121.

[41] M. Gong, M. Gong, Y. Li, H. Wang, Y. Liang, J.Z. Wu, J. Zhou, J. Wang, T. Regier, F. Wei, H. Dai, An advanced Ni-Fe layered double hydroxide electrocatalyst for water oxidation, J. Am. Chem. Soc. 135 (2013) 8452–8455 31.

[42] X. Lu, C. Zhao, Electrodeposition of hierarchically structured three-dimensional nickel-iron electrodes for efficient oxygen evolution at high current densities, Nat. Commun. 6 (2015) 6616.

[43] D. Friebel, M.W. Louie, M. Bajdich, K.E. Sanwald, Y. Cai, A.M. Wise, M.-J. Cheng, D. Sokaras, T.-C. Weng, R. Alonso-Mori, R.C. Davis, J.R. Bargar, J.K. Norskov, A. Nilsson, A.T Bell, Identification of highly active Fe sites in (Ni,Fe)OOH for electrocatalytic water splitting, J. Am. Chem. Soc. 137 (2015) 1305–1313.